View metadata, citation and similar papers at core.ac.uk

brought to you by CORE

provided by University of Regensburg Publication Server

Dynamic nuclear spin polarization in an all-semiconductor spin injection device with (Ga,Mn)As/n-GaAs spin Esaki diode

J. Shiogai, M. Ciorga, M. Utz, D. Schuh, T. Arakawa, M. Kohda, K. Kobayashi, T. Ono, W. Wegscheider, D. Weiss, and J. Nitta

Citation: Applied Physics Letters **101**, 212402 (2012); doi: 10.1063/1.4767339

View online: http://dx.doi.org/10.1063/1.4767339

View Table of Contents: http://scitation.aip.org/content/aip/journal/apl/101/21?ver=pdfcov

Published by the AIP Publishing

Articles you may be interested in

In-plane tunneling anisotropic magnetoresistance in (Ga,Mn)As/GaAs Esaki diodes in the regime of the excess current
Appl. Phys. Lett. **106**, 262402 (2015); 10.1063/1.4923309

Local spin valve effect in lateral (Ga,Mn)As/GaAs spin Esaki diode devices
AIP Advances **1**, 022113 (2011); 10.1063/1.3591397

Manipulation of nuclear spin dynamics in n-GaAs using an on-chip microcoil
J. Appl. Phys. **109**, 016106 (2011); 10.1063/1.3530731

Tunneling anisotropic spin polarization in lateral (Ga,Mn)As/GaAs spin Esaki diode devices
Appl. Phys. Lett. **95**, 152101 (2009); 10.1063/1.3247187

Bias voltage dependence of the electron spin injection studied in a three-terminal device based on a (Ga , Mn) As ⁄ n + - Ga As Esaki diode
Appl. Phys. Lett. **89**, 012103 (2006); 10.1063/1.2219141

Reuse of AIP Publishing content is subject to the terms at: https://publishing.aip.org/authors/rights-and-permissions. Download to IP: 132.199.145.239 On: Mon, 24 Oct 2016 11:22:58

Dynamic nuclear spin polarization in an all-semiconductor spin injection device with (Ga,Mn)As/*n*-GaAs spin Esaki diode

J. Shiogai,[1,2,3] M. Ciorga,[2] M. Utz,[2] D. Schuh,[2] T. Arakawa,[3] M. Kohda,[1,4] K. Kobayashi,[3] T. Ono,[3] W. Wegscheider,[2,5] D. Weiss,[2] and J. Nitta[1]
[1]*Department of Materials Science, Tohoku University, 980-8579 Sendai, Miyagi, Japan*
[2]*Institute of Experimental and Applied Physics, University of Regensburg, D-93040 Regensburg, Germany*
[3]*Institute for Chemical Research, Kyoto University, 611-0011 Uji, Kyoto, Japan*
[4]*PRESTO, Japan Science and Technology Agency, 332-0012 Kawaguchi, Saitama, Japan*
[5]*Department of Physics, ETH Zürich, 8093 Zürich, Switzerland*

(Received 12 October 2012; accepted 30 October 2012; published online 21 November 2012)

We investigate the dynamic nuclear spin polarization in an *n*-GaAs lateral channel induced by electrical spin injection from a (Ga,Mn)As/*n*-GaAs spin Esaki diode. Signatures of nuclear spin polarization are studied in both three-terminal and non-local voltage signals, where a strong electron spin depolarization feature is observed close to zero magnetic field. This is due to the large nuclear field induced in the channel through hyperfine interaction between injected electron spins and localized nuclear spins. We study the time evolution of the dynamic nuclear spin polarization and evaluate polarization and relaxation times of nuclear spins in the channel. © *2012 American Institute of Physics*. [http://dx.doi.org/10.1063/1.4767339]

Electrical spin injection from ferromagnets to lateral semiconductor structures[1,2] makes it possible to investigate a variety of physical phenomena relevant to nuclear spins by all electrical means,[3,4] which so far have only been studied in nanostructures at high magnetic fields,[5] in the quantum Hall regime,[6–8] and by optical means.[9–12] Recent works focused on dynamic nuclear spin polarization (DNP) effects,[3,4] occurring as a result of strong coupling between spin-polarized electrons and lattice nuclei through hyperfine interaction. The reason for this is that thanks to DNP, an all-electrical initialization and manipulation of nuclear spins, potentially useful for future quantum computing, could be easily done by electrical spin injection. The nuclear spin polarization and nuclear magnetic resonance (NMR) have been intensively studied in ferromagnetic metal/semiconductor hybrid structures with a Schottky barrier junction.[3,4] The spin injection efficiency in these devices was on the order of a few percent, thus enabling only static investigations of the nuclear spin polarization due to the weak hyperfine interaction. (Ga,Mn)As/*n*-GaAs spin Esaki diodes on the other hand showed high spin injection efficiency exceeding 50% at low bias[2] owing to the high spin polarization of (Ga,Mn)As.[16,17] While a full theoretical understanding of DNP in all-electrical spin injection devices with lateral structures has not fully been established yet, the nuclear magnetic field is proportional to the spin polarization of electrons in the channel $P_N = (n_\uparrow - n_\downarrow)/(n_\uparrow + n_\downarrow) = \Delta\mu D(E_F)/n$, where n_σ denotes total carrier concentration with up and down spins, respectively, and $\Delta\mu$ and $D(E_F)$ are spin splitting of the Fermi level and density of states at the Fermi energy, respectively. Here P_N, which decays with distance from the spin injector, can be described by the product of spin injection efficiency P_{inj} and spin injection current I_{inj} as follows:[18]

$$P_N(x) = P_N(0)\exp\left(-\frac{x}{\lambda_{sf}}\right) = \frac{3\rho_N\lambda_{sf}P_{inj}I_{inj}}{2SE_F}\exp\left(-\frac{x}{\lambda_{sf}}\right), \quad (1)$$

with ρ_N, S, λ_N being resistivity and cross-sectional area of the channel and electron spin diffusion length in the channel, respectively. Since the spin Esaki diode provides high spin injection efficiency at relatively high bias voltages, these structures could lead to a more efficient nuclear spin polarization and manipulation compared to metal/semiconductor hybrid structures. This enables us, e.g., to investigate the time evolution of the nuclear spin polarization. In this letter, we present the time evolution of nuclear spin polarization and depolarization as well as NMR studies in an all-semiconductor spin injection device with the (Ga,Mn)As/*n*-GaAs Esaki diode spin polarizers[13–15] and detectors using both non-local spin-valve (NLSV) and local three-terminal (3T) techniques.

A spin injection device was fabricated from an epitaxial wafer, grown by molecular beam epitaxy, consisting of semi-insulating GaAs, 300 nm GaAs buffer layer, 500 nm AlGaAs/GaAs superlattice, 1-μm-thick *n*-GaAs followed by 15 nm of GaAs with linearly graded doping $n \rightarrow n^+$ with $n = 2.5 \times 10^{16}\,\mathrm{cm}^{-3}$ and $n^+ = 6.0 \times 10^{18}\,\mathrm{cm}^{-3}$, 8 nm n^+-GaAs, 2.2 nm AlGaAs diffusion barrier and finally 50 nm (Ga,Mn)As. A 10-μm-wide mesa, oriented along the [010] GaAs direction, is used as a transport channel where six (Ga,Mn)As/*n*-GaAs spin Esaki junctions, defined by electron beam lithography and reactive ion etching, constitute spin-injection and detection contacts (see Fig. 1(a)). The distances between contact 2 and contacts 3, 4, 5 are 5, 20, and 25 μm, respectively. In the experiments, the four contacts in the middle (contacts 2–5) in the size of $1 \times 10\,\mu\mathrm{m}^2$ are used as spin injectors or detectors while contacts 1 and 6 serve as reference electrodes. All measurements are performed at $T = 4$ K, which is much lower than the ferromagnetic transition temperature of the (Ga,Mn)As electrodes. An easy axis of (Ga,Mn)As is in-plane parallel to the ⟨100⟩ direction.

First, we demonstrate electrical spin injection into the GaAs channel by measuring NLSV and also Hanle effect, i.e., the depolarization of spin accumulation by a perpendicular external magnetic field. The filled and open black symbols in

 © 2012 American Institute of Physics

Reuse of AIP Publishing content is subject to the terms at: https://publishing.aip.org/authors/rights-and-permissions. Download to IP: 132.199.145.239 On: Mon, 24 Oct 2016 11:22:58

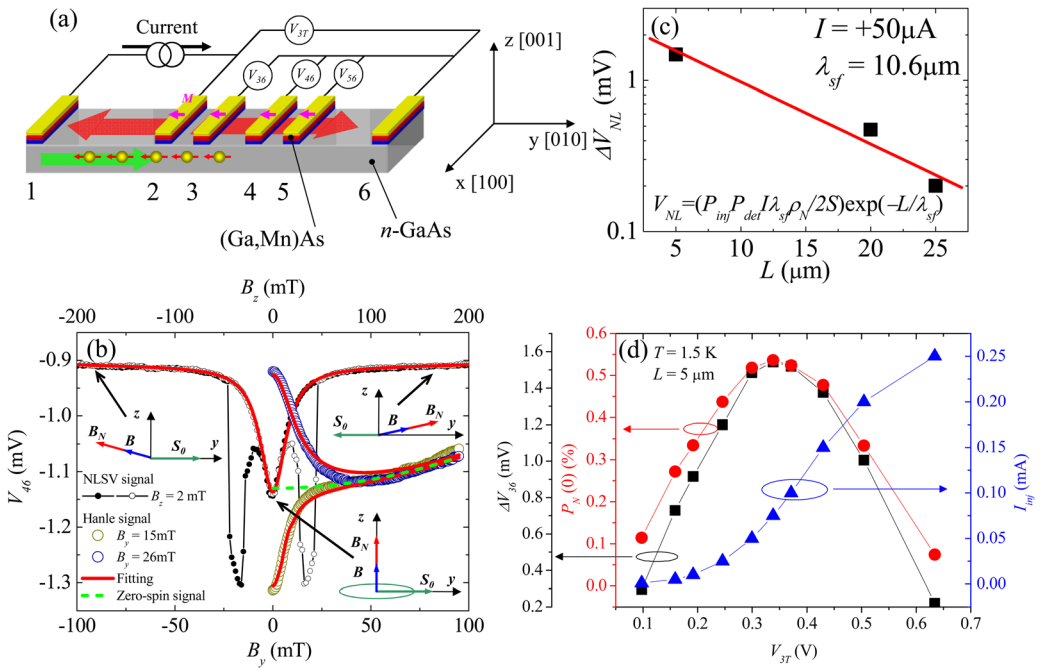

FIG. 1. (a) Schematic diagram of the sample (not to scale) and coordinate system. Local voltage V_{3T} is measured between contacts 2 and 6 by three-terminal method with a spin injection current applied from contacts 1 to 2, while non-local voltages V_{36}, V_{46}, V_{56} are measured between contacts 3, 4, 5, and contact 6. (b) The NLSV signal as a function of B_y swept from positive to negative saturation field (open black symbols) and back (closed black symbols) with $B_z = 2$ mT. Hanle signal taken by the non-local voltage is shown as a function of B_z for parallel ($B_y = 26$ mT, open blue circles) and antiparallel ($B_y = 15$ mT, open yellow circles) contact magnetization configuration. Red lines show the best fitting results of the data with Eq. (3). Insets show the relative directions of electron and nuclear spins. (c) The amplitude of NLSV signal, defined as difference of non-local voltages between in parallel and anti-parallel magnetization configuration, as function of injector-detector separation. (d) The amplitude of NLSV signal at the contact 3 (black squares), calculated spin polarization below the injector (red circles), and spin injection current (blue triangles) as a function of 3T bias voltage across the spin injector.

Fig. 1(b) show a typical NLSV trace as a function of the in-plane magnetic field B_y (bottom horizontal axis in Fig. 1(b)) under the spin injection current $I_{21} = +50\,\mu$A. This positive bias corresponds to the spin extraction resulting in a spin accumulation in the *n*-GaAs channel. For NLSV measurements, a small $B_z = 2$ mT is applied normal to the surface to polarize nuclear spins along the z-direction near $B_y = 0$ mT. The non-local voltage V_{46} shows abrupt voltage changes around $B_y = 13$ mT and 21 mT, ascribed to a switching between parallel ($V_{\uparrow\uparrow}$) and anti-parallel ($V_{\uparrow\downarrow}$) alignment of injector and detector magnetizations. In contrast to previous measurements of the NLSV signal,[2] the present sample shows complete parallel and anti-parallel magnetization configurations due to enhanced strain-induced uniaxial anisotropy along the easy axis in [100] direction.[19] From the amplitude $\Delta V = V_{\uparrow\uparrow} - V_{\uparrow\downarrow}$ of the NLSV signal and its distance dependence, we obtain the spin injection and detection efficiencies of 4.1% and 57%, respectively, and a spin relaxation length of 10.6 μm for $I_{21} = +50\,\mu$A (see Ref. 2 for more details). Figs. 1(c) and 1(d) summarize distance and bias dependence of the signal amplitude ΔV and spin polarization in the channel P_N, with the latter calculated using Eq. (1). Both ΔV and P_N are proportional to the product of spin injection efficiency and spin injection current, with the former dropping rapidly with increasing bias voltage.[2] As a result, they both show maximum values for a current range from around +50 up to around 100 μA, which for electron spin polarization underneath the spin injector reaches $P_N(0) = 52\%$. The above current values were then chosen for most of the following experiments because of the efficient hyperfine interaction. Around $B_y = 0$ mT, the depolarization dip due to the DNP is clearly observed. The voltage value $V_0 = -1.14$ mV measured at $B_y = 0$ mT is half way between $V_{\uparrow\uparrow}$ (−1.30 mV) and $V_{\uparrow\downarrow}$ (−0.91 mV). According to the standard equation of the NLSV signals,[18] this voltage corresponds to the zero spin signal. Therefore, the measured V_0 constitutes the background signal, commonly measured in NLSV measurements.[1,2]

The electron spin depolarization is further confirmed by measuring the non-local voltage as a function of the perpendicular magnetic field B_z shown by blue and yellow circles in Fig. 1(b). These Hanle curves, obtained at $B_y = 15$ mT (parallel magnetization) and 26 mT (anti-parallel magnetization), are plotted in the same figure as the NLSV signal but as a function of B_z (top horizontal axis in Fig. 1(b)). At sufficiently large B_z, where injected electron spins are completely depolarized, the non-local voltage drops to the background value V_0 which shows a quadratic dependence on B_z (green-dashed line in Fig. 1(b)).[2] We do not observe the so-called Hanle oscillations,[20] since they are suppressed by the applied in-plane magnetic field.

The origin of the depolarization curve was discussed in Ref. 8. In the presence of hyperfine interaction between nuclear and electron spins, the total magnetic fields acting on the electron spins are the sum of the applied external magnetic field $\boldsymbol{B}$ and the internal nuclear magnetic field $\boldsymbol{B_N}$. In steady state, the latter can be expressed as[21]

$$\boldsymbol{B}_N = fb_N \frac{\boldsymbol{B} \cdot \langle \boldsymbol{S} \rangle}{B^2} \boldsymbol{B} \tag{2}$$

assuming that the Knight field and local dipole fields are negligibly small. Here, the electron spin polarization $\langle S \rangle$ is equal to 1/2 when the electron spins are fully polarized. The average spin polarization $\langle S \rangle$ can be replaced by the spin polarization in the channel, as given by Eq. (1), divided by 2.

Reuse of AIP Publishing content is subject to the terms at: https://publishing.aip.org/authors/rights-and-permissions. Download to IP: 132.199.145.239 On: Mon, 24 Oct 2016 11:22:58

The value of b_N was calculated to be -17 T in bulk n-GaAs and typical value of fb_N is experimentally measured to be -1.7 T.[21] According to Eq. (2), $\boldsymbol{B_N}$ is oriented either parallel or antiparallel to $\boldsymbol{B}$ depending on the direction of electron spins. This is illustrated by the simple vector diagrams in Fig. 1(b) for different B_y values. At $B_y = 0$ mT, the nuclear field $\boldsymbol{B_N}$ is oriented along the z-axis due to the small applied B_z. Since large B_N causes a fast precession of electron spins in the xy-plane, in-plane spin components are averaged to zero. From Eq. (2), we evaluate the strength of $\boldsymbol{B_N}$ underneath the contact 4 to be 65.5 mT using the spin polarization P_N of 51.8% and λ_{sf} of 10.6 μm obtained from NLSV measurements at $I_{21} = +50$ μA. The induced nuclear field is large enough for the electron spins to start the precession. Therefore, the electron spin polarization along $\boldsymbol{B_N}$ is reduced by a factor of cosα with α being the angle between $\boldsymbol{B}$ and $\boldsymbol{B}_y$. Since the ferromagnetic contact detects a spin polarization projected onto its magnetization direction, i.e., the y-direction in the present configuration, the spin signal $V_{46} - V_0$ can be fitted with

$$V_{NL} - V_0 \sim \langle S_0 \rangle \cos^2\alpha \sim \frac{B_y^2}{B_y^2 + B_z^2 + \Delta B^2}, \qquad (3)$$

where ΔB corresponds to the half width at half maximum of the Lorentz curve $\sim(1 + \Delta B^2/B_y^2)^{-1}$ when $B_z = 0$ mT.[3] Since the nuclear spins are polarized in both NLSV and Hanle effect geometries, Eq. (3) can be applied for both configurations using ΔB as free parameter. The best fits for both NLSV and the Hanle type curves using Eq. (3) are shown in Fig. 1(b) as solid red lines. For both cases, we obtain a small correction term $\Delta B \sim 5$ mT. This suggests that a field perpendicular to the swept field is present in the sample when the latter is swept across the zero. In. Ref. 3, such field is attributed to dipole-dipole interactions between nuclear spins. Generally, all these experiments demonstrate that the nuclear field can be well controlled by a small external magnetic field in accordance with Eq. (2).

To further confirm a coupling of electron and nuclear spins, we performed NMR studies. During these measurements, an oblique static external magnetic field B_{yz} was applied at an angle of 15° with respect to the y-axis in the yz-plane, while the ac field was aligned along the x-axis perpendicular to the static one. Figure 2(a) shows a frequency scan of the non-local voltage V_{36} at different strengths of $B_{yz} = -43.0$ mT, -34.9 mT, and -26.7 mT. When the ac magnetic field is not at resonance, all nuclear spin species and electron spins are polarized along the external magnetic field. At resonance, the corresponding nuclear spins start to rotate and acquire an angle with the electron spins, resulting in precession of electron spins along the reoriented nuclear field.[22] As a result, the component of electron spins along the external magnetic field is reduced, leading to reduced voltages. We observed such NMR signals both in NLSV and 3T configurations. Resonance frequencies obtained from three-terminal voltages, V_{3T}, and three different non-local voltages V_{36}, V_{46}, and V_{56} increase linearly with the external magnetic field as is summarized in Fig. 2(b). From the linear slope of the resonant frequency shift with the magnetic field, three resonance peaks in Fig. 2(a) are identified as single

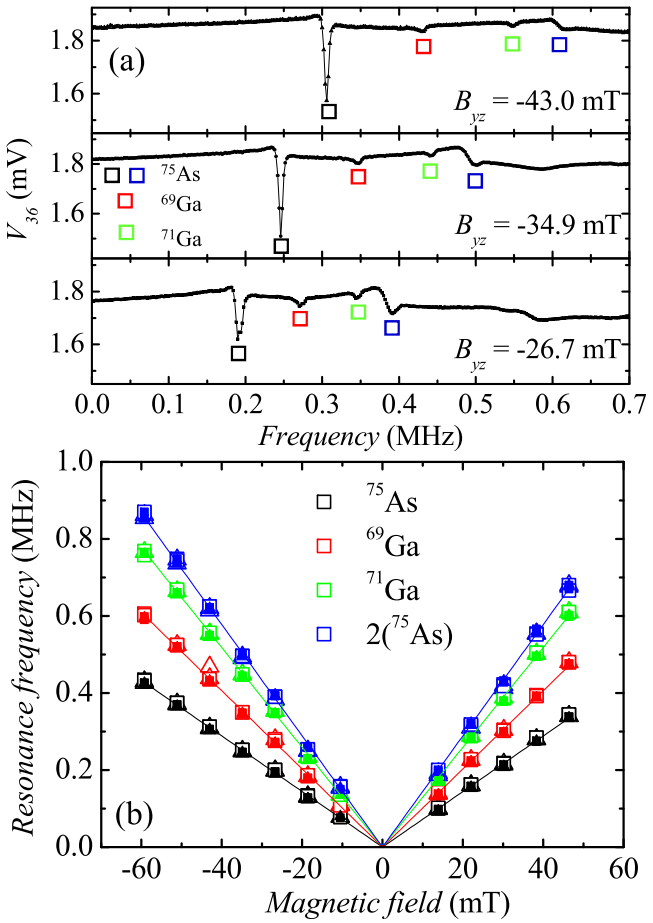

FIG. 2. (a) NMR spectrum at different static fields $B_{yz} = -43.0$ mT, -34.9 mT, -26.7 mT. Different colored symbols represent resonance peaks of different nuclear species. (b) Resonance frequencies as a function of external magnetic field for all spin detectors, i.e., V_{3T} (open triangles), V_{36} (open squares), V_{46} (filled triangles), and V_{56} (filled squares).

spin resonances of the three main isotopes ^{75}As, ^{69}Ga, and ^{71}Ga, while the fourth one corresponds to the second-order resonance of the isotope ^{75}As. The resulting gyromagnetic ratios of 4.53 ± 0.015, 6.38 ± 0.017, 8.14 ± 0.016, and $9.07 \pm 0.015 \times 10^7$ rad/Ts for ^{75}As, ^{69}Ga, ^{71}Ga, and 2(^{75}As) resonances are in good agreement with the reported values corresponding to 4.596, 6.450, 8.196, and 9.192×10^7 rad/Ts.[23] These NMR measurements provide clear evidence that polarized nuclear spins get electrically detected.

Finally and most importantly, we investigated the time evolution of polarization and relaxation of nuclear spins in accordance with investigations on spin-LEDs.[11,12] In the measurement, the external magnetic field B_{yz} was aligned 15° off the y-direction and the time evolution of the V_{3T} voltage was monitored. In Fig. 3(a), we plot the three-terminal resistance R_{3T} defined as V_{3T}/I_{21} measured while sweeping B_{yz} from negative to positive values with $I_{21} = +50$ μA. We clearly observe a jump at $B_{yz} \sim 15$ mT related to the magnetization switching in the contact and a depolarization peak around $B_{yz} = 0$ mT indicating the clear evidence of DNP. The time evolution measurements are performed at $B_{yz} = 2.34$ mT, indicated with a black dashed line in Fig. 3(a), in the following way: First, B_{yz} is swept from a negative saturation field through zero up to 2.34 mT with the current off condition in order to obtain antiparallel alignment between the

Reuse of AIP Publishing content is subject to the terms at: https://publishing.aip.org/authors/rights-and-permissions. Download to IP: 132.199.145.239 On: Mon, 24 Oct 2016 11:22:58

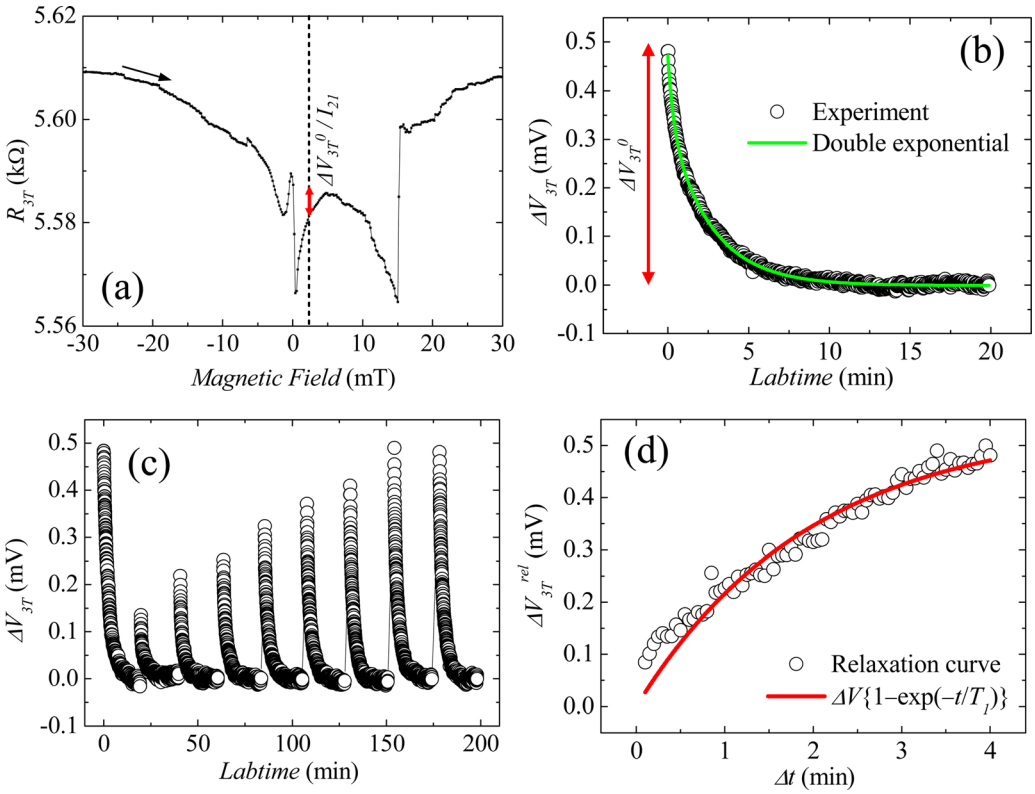

FIG. 3. (a) Three terminal resistance R_{3T} obtained for $I_{inj} = +50\,\mu$A under oblique external magnetic field, 15° off from the y-axis in the yz-plane. The red arrow shows the resistance change due to nuclear spin polarization, corresponding to the initial value of ΔV_{3T}^0, as indicated in (b) (see text for details). (b) Time evolution of the nuclear spin polarization (black open symbol) at $B_{yz} = 2.34$ mT and corresponding fit using Eq. (4) (green line). (c) V_{3T} as a function of laboratory time at $B_{yz} = 2.34$ mT in $I_{inj} = +104\,\mu$A for 20 min and subsequently switching it off with different Δt steps (see text). For clarity, only some typical polarization curves are shown. (d) Relaxation curve of nuclear spins as a function of switch-off time Δt (open black circles) with corresponding fit (red line) based on Eq. (5).

magnetization of the (Ga,Mn)As spin injector and the in-plane component of the external magnetic field. After that, the injection current I_{21} is turned on to accumulate electron spins underneath the contact, which increases the measured V_{3T}. As a result of the spin injection, the DNP is generated so that the precession and depolarization of the injected electron spins are induced due to the nuclear field. Such an electron spin dynamics is reflected by the time evolution of the measured V_{3T} which decreases as the nuclear polarization builds up and saturates after a certain time interval at a value corresponding to the saturation nuclear field for a given experimental condition. In Fig. 3(b), we plot the time evolution of the voltage change $\Delta V_{3T} = V_{3T} - V_{3T}^{sat}$, where V_{3T}^{sat} is the voltage measured at saturation for $I_{21} = +104\,\mu$A. As can be seen in Fig. 1(d), the spin polarization P_N shows a value close to maximum at this spin injection current. In Fig. 3(a), the red arrow indicates the maximum voltage change ΔV_{3T}^0 with respect to the initial value. Hence, the curve in Fig. 3(b) gives us the information about the time evolution of the nuclear polarization. We find that the time evolution curve can be well fitted with a double exponential decay of the form

$$\Delta V_{3T} = V_1 \exp(-t/\tau_1) + V_2 \exp(-t/\tau_2). \quad (4)$$

From a fit, we obtain $\tau_1 = 20.9 \pm 0.7$ s and $\tau_2 = 158.7 \pm 1.0$ s with V_1 and V_2 being 0.13 and 0.34 mV, respectively. The two different polarization times may be due to the different mechanism behind the polarization dynamics, e.g., regular hyperfine interaction and nuclear spin diffusion. According to previous reports, the latter mechanism needs to be taken into account also for nuclear spin relaxation.[24] To measure the relaxation of nuclear spins, we first apply the current for a time long enough to saturate the DNP signal, switch off the current for a time interval Δt, and then monitor the signal after switching the current back on. Figure 3(c) shows some of the experimental curves displaying V_{3T} as a function of laboratory time with different off-state times Δt applying, as before, $B_{yz} = 2.34$ mT and an injection current $I_{21} = +104\,\mu$A. The whole set of curves was obtained as follows: (i) the spin injection current was switched on for 20 min and a nuclear polarization build-up curve, similar to the one in Fig. 3(b), was obtained; (ii) I_{21} was switched off for a time interval Δt; (iii) the current was switched back on to repeat (i) and (ii) but with Δt increased by 3 s. Every time after switching off the current, nuclear spins relax during the time interval Δt and the electron spin polarization partially recovers. This is reflected in the initial value V_{3T}^{ini} of the three-terminal voltage measured immediately after switching the current on again, which is increased by ΔV_{3T}^{rel} with respect to the saturation value V_{3T}^{sat} measured before switching the current off. ΔV_{3T}^{rel} is then a measure of the relaxation of nuclear spins with time Δt. Figure 3(d) shows the dependence of ΔV_{3T}^{rel} on Δt, which can be well fitted with

$$\Delta V_{3T}^{rel} = V_{3T}^{ini} - V_{3T}^{sat} = \Delta V_{3T}^0 \{1 - \exp(-t/T_1)\}, \quad (5)$$

Reuse of AIP Publishing content is subject to the terms at: https://publishing.aip.org/authors/rights-and-permissions. Download to IP: 132.199.145.239 On: Mon, 24 Oct 2016 11:22:58

where T_1 represents the spin lattice relaxation time of nuclear spins. From the fit, we obtained a spin lattice relaxation time of 117 s. Such a time scale on the order of minutes is consistent with optically detected NMR measurements in bulk *n*-GaAs[25] and ten times shorter than the nuclear spin relaxation time in depleted GaAs.[26] We ascribe the difference with respect to the latter experiment to the fact that in our case, hyperfine interaction of nuclear spins with surrounding electrons dominates the nuclear spin relaxation, while in the case of depleted GaAs nuclear spin diffusion is the dominant mechanism.[26]

In conclusion, we have clearly demonstrated the presence of DNP in lateral all-semiconductor structures through the observed depolarization signature in NLSV that can be explained by a dynamically polarized nuclear field. The NMR experiment revealed that all possible nuclear species in the present experiments were polarized. We also demonstrated the time evolution of nuclear spin polarization and relaxation in the NLSV device in *n*-GaAs channel. Time evolution of the DNP was able to be observed due to the high spin injection efficiency from the (Ga,Mn)As/*n*-GaAs spin Esaki diode, promising the effective initialization and manipulation of nuclear field with a small external magnetic field.

This work was partly supported by the German Science Foundation (DFG) via SFB 689, the Japan-Germany Strategic International Cooperative Program (Joint Research Type) from JST and DFG (FOR 1483), Grants-in-Aid from JSPS, MEXT, and the Collaborative Research Program of Institute for Chemical Research, Kyoto University (Grant # 2011-75).

[1]X. Lou, C. Adelmann, S. A. Crooker, E. S. Garlid, J. Zhang, K. S. Madhukar Reddy, S. D. Flexner, C. J. Palmstrøm, and P. A. Crowell, Nat. Phys. **3**, 197 (2007).
[2]M. Ciorga, A. Einwanger, U. Wurstbauer, D. Schuh, W. Wegscheider, and D. Weiss, Phys. Rev. B **79**, 165321 (2009).
[3]G. Salis, A. Fuhrer, and S. F. Alvarado, Phys. Rev. B **80**, 115332 (2009).
[4]M. K. Chan, Q. O. Hu, J. Zhang, T. Kondo, C. J. Palmstrøm, and P. A. Crowell, Phys. Rev. B **80**, 161206(R) (2009).
[5]G. Yusa, K. Muraki, K. Takashina, K. Hashimoto, and Y. Hirayama, Nature **434**, 1001 (2005).
[6]D. C. Dixon, K. R. Wald, P. L. McEuen, and M. R. Melloch, Phys. Rev. B **56**, 4743 (1997)
[7]T. Machida, T. Yamazaki, K. Ikushima, and S. Komiyama, Appl. Phys. Lett. **82**, 409 (2003).
[8]M. Kawamura, H. Takahashi, K. Sugihara, S. Masubuchi, K. Hamaya, and T. Machida, Appl. Phys. Lett. **90**, 022102 (2007).
[9]H. Sanada, Y. Kondo, S. Matsuzaka, K. Morita, C. Y. Hu, Y. Ohno, and H. Ohno, Phys. Rev. Lett. **96**, 067602 (2006).
[10]J. Strand, B. D. Schultz, A. F. Isakovic, C. J. Palmstrøm, and P. A. Crowell, Phys. Rev. Lett. **91**, 036602 (2003).
[11]P. Van Dorpe, W. Van Roy, J. De Boeck, and G. Borghs, Phys. Rev. B **72**, 035315 (2005).
[12]J. Strand, X. Lou, C. Adelmann, B. D. Schultz, A. F. Isakovic, C. J. Palmstrøm, and P. A. Crowell, Phys. Rev. B **72**, 155308 (2005).
[13]M. Kohda, Y. Ohno, K. Takamura, F. Matsukura, and H. Ohno, Jpn. J. Appl. Phys., Part 2 **40**, L1274 (2001).
[14]E. Johnston-Halperin, D. Lofgreen, R. K. Kawakami, D. K. Young, L. Coldren, A. C. Gossard, and D. D. Awschalom, Phys. Rev. B **65**, 041306 (2002).
[15]P. Van Dorpe, Z. Liu, W. Van Roy, V. F. Motsnyi, M. Sawicki, G. Borghs, and J. De Boeck, Appl. Phys. Lett. **84**, 3495 (2004).
[16]T. Ogawa, M. Shirai, N. Suzuki, and I. Kitagawa, J. Magn. Magn. Mater. **196–197**, 428 (1999).
[17]D. Chiba, F. Matsukura, and H. Ohno, Physica E **21**, 966 (2004).
[18]T. Takahashi and S. Maekawa, Phys. Rev. B **67**, 052409 (2003).
[19]J. Wenisch, C. Gould, L. Ebel, J. Storz, K. Pappert, M. J. Schmidt, C. Kumpf, G. Schmidt, K. Brunner, and L. W. Molenkamp, Phys. Rev. Lett. **99**, 077201 (2007).
[20]J. Li, B. Huang, and I. Appelbaum, Appl. Phys. Lett. **92**, 142507 (2008).
[21]D. Paget, G. Lampel, B. Sapoval, and V. I. Safarov, Phys. Rev. B **15**, 5780 (1977).
[22]G. P. Flinn, R. T. Harley, M. J. Snelling, A. C. Tropper, and T. M. Kerr, J. Luminescence **45**, 218 (1990).
[23]R. R. Ernst, G. Bodenhausen, and A. Wokaun, *Principles of Nuclear Magnetic Resonance in One and Two Dimensions* (Oxford University Press, Oxford, 1987).
[24]T. Nakajima, Y. Kobayashi, S. Komiyama, M. Tsuboi, and T. Machida, Phys. Rev. B **81**, 085322 (2010).
[25]D. Paget, Phys. Rev. B **25**, 4444 (1982).
[26]K. Hashimoto, K. Muraki, T. Saku, and Y. Hirayama, Phys. Rev. Lett. **88**, 176601 (2002).

Reuse of AIP Publishing content is subject to the terms at: https://publishing.aip.org/authors/rights-and-permissions. Download to IP: 132.199.145.239 On: Mon, 24 Oct 2016 11:22:58